

Photoluminescence properties of Sm^{3+} -doped $\text{ZrO}_2\text{-TiO}_2\text{-Al}_2\text{O}_3$ coatings

Stancho Yordanov*, Bojidar Jivov, Vladimir Petkov, Shaban Uzun, Mihaela Aleksandrova

Bulgarian Academy of Sciences, Institute of Metal Science, Equipment and Technologies with Hydro- and Aerodynamics Centre

“Acad. A. Balevski”, 67 “Shipchenski prohod” Blvd., 1574 Sofia, Bulgaria

e-mail: stancho14@abv.bg

Abstract: The emission spectrum of the $\text{ZrO}_2\text{-TiO}_2\text{-Al}_2\text{O}_3\text{-Sm}_2\text{O}_3$ coating was recorded at different excitation wavelengths. Under UV excitation ($\lambda_{\text{ex}} = 354 \text{ nm}$), broad band with a maximum around 420–440 nm was observed and can be associated with oxygen vacancies in ZrO_2 together with Ti^{3+} centers. Weakly intense and narrower emission bands at 600 nm and 647 nm are assigned to the ${}^5\text{G}_{5/2} \rightarrow {}^7\text{H}_{7/2}$ and ${}^5\text{G}_{5/2} \rightarrow {}^7\text{H}_{9/2}$ transitions of Sm^{3+} ions. Under excitation with 404 nm the emission is dominated by defect levels in the oxide coating. The values of the chromaticity coordinates of the coating excited under 354 nm correspond to the pale pink color of emission (0.252, 0.272) and under 404 nm has orange color of emission (0.353, 0.370).

Keywords: EMISSION SPECTRUM, SOL-GEL METHOD, DIP COATING, $\text{ZrO}_2\text{-TiO}_2\text{-Al}_2\text{O}_3\text{-Sm}_2\text{O}_3$

1. Introduction

The use of oxide coatings is a classic technological approach for effective protection or modification of the characteristics of the working surface of various technical parts and finished products [1-4]. Coatings with increased chemical, corrosion and thermal resistance, high hardness and wear resistance, suitable optical properties, adequate biocompatibility and other performance indicators are widely used [5-11]. Various technological approaches have been developed for the deposition of functional coatings. In this aspect, a number of methods are applicable: [12-22]: physical vapor deposition (PVD), chemical vapor deposition (CVD), combustion synthesis, micro-arc oxidation, laser cladding, plasma spraying, sol-gel technique and a number of others.

Ceramic materials with increased Al_2O_3 content exhibit good wear resistance and friction, as well as stable chemical properties [23-28]. On the other hand, in some product categories, relative brittleness, inadequate thermal shock resistance, tendency to stress concentration and crack formation, as well as other operational problems are observed [29]. The development of optimized compositions based on Al_2O_3 in combination with other oxide components allows the production of coatings with appropriate phase composition, adequate microstructure and functional characteristics [25-28].

The mechanical properties and oxidation resistance of multilayer thermal barrier coatings $\text{Al}_2\text{O}_3/\text{ZrO}_2$ prepared by plasma-sprayed method were investigated [30]. Nanocomposite coatings $\text{Al}_2\text{O}_3\text{-ZrO}_2$ were prepared, which showed lower porosity and higher values for toughness and microhardness than those found for monophase coatings of Al_2O_3 or ZrO_2 [31,32]. At the same time, lower thermal conductivity was registered for $\text{Al}_2\text{O}_3\text{-ZrO}_2$ coatings than for Al_2O_3 samples [31].

Compared to Al_2O_3 , the titanium dioxide TiO_2 is characterized by smaller brittleness and a number of favorable technological properties, therefore it is considered as a suitable oxide component applicable in the development of binary and more complex compositions. The effect of the introduction of TiO_2 to Al_2O_3 -based oxide coatings on the microstructure and operational properties of the experimental samples has been analyzed [33].

The role of the composition and tribological behavior in the prepared coatings with a change in the TiO_2 content has been studied [34]. With $\text{Al}_2\text{O}_3/\text{TiO}_2$ coating, higher wear resistance was registered than that found with Al_2O_3 coating [35]. It has been established that the reinforcement with TiO_2 of the composite coating $\text{Al}_2\text{O}_3\text{-3\%TiO}_2$ provides more favorable tribological properties than the reinforcement with zirconium dioxide ZrO_2 [36].

It has been proven that the $\text{Al}_2\text{O}_3\text{-40\%TiO}_2$ coatings have a higher wear resistance than the $\text{Al}_2\text{O}_3\text{-13\%TiO}_2$ oxide coatings. With an increase in the content of the introduced TiO_2 in the $\text{Al}_2\text{O}_3\text{-TiO}_2$ coatings, a decrease in porosity and the presence of cracks was found, and at the same time, an increase in tightness and the corrosion resistance [37]. At the $\text{Al}_2\text{O}_3\text{-40\%TiO}_2$ coating, a higher microhardness was registered compared to that found at the substrate used [38].

In the ternary oxide system $\text{Al}_2\text{O}_3\text{-ZrO}_2\text{-TiO}_2$, a series of composite coatings and a comparative two-component sample were obtained. The effect of introducing 2 wt%, 6 wt% and 10 wt% TiO_2 to the composition of eutectic $\text{Al}_2\text{O}_3\text{-ZrO}_2$ (at 6:4 molar ratio) on the properties of the samples, microstructure and change in the phase composition was analyzed [29]. Composite powders (by spray granulation) were obtained from the prepared compositions, which were deposited on substrates by plasma spraying.

The presence of the crystalline phases t- ZrO_2 , $\alpha\text{-Al}_2\text{O}_3$, m- ZrO_2 and TiO_2 (in rutile form) was proven in the obtained composite powders. At the prepared composite coatings ($\text{Al}_2\text{O}_3\text{-ZrO}_2\text{-TiO}_2$) only the crystalline phases t- ZrO_2 , $\alpha\text{-Al}_2\text{O}_3$, $\gamma\text{-Al}_2\text{O}_3$ and amorphous phase were registered [29]. At the studied coatings, the diffraction peaks of TiO_2 were not observed, even in compositions with a content of 10 wt% TiO_2 . Due to the specificity of the used technological approach and extremely high undercooling, an amorphous phase is formed in the obtained $\text{Al}_2\text{O}_3\text{-ZrO}_2\text{-TiO}_2$ coatings. It is assumed that a probable dissolution of TiO_2 in the amorphous phase or the formation of a solid solution together with $\gamma\text{-Al}_2\text{O}_3$ occurs during the cooling period [29].

With increasing TiO_2 content, a decrease in the porosity of the prepared $\text{Al}_2\text{O}_3\text{-ZrO}_2\text{-TiO}_2$ coatings was observed. At a concentration of 10 wt% TiO_2 (with $\text{Al}_2\text{O}_3\text{-ZrO}_2\text{-TiO}_2$ coating), a dense and uniform microstructure and higher values of adhesive strength, toughness and microhardness were found than those found for the comparative $\text{Al}_2\text{O}_3\text{-ZrO}_2$ coating. For an experimental sample with the composition $\text{Al}_2\text{O}_3\text{-ZrO}_2\text{-10wt\%TiO}_2$, the adhesive strength of 25.38 MPa was registered, while for $\text{Al}_2\text{O}_3\text{-ZrO}_2$ coating, a value of 21.50 MPa was found [29]. It has been proven that the obtained three-component oxide coating $\text{Al}_2\text{O}_3\text{-ZrO}_2\text{-TiO}_2$ (with a content of 10 wt% TiO_2) has a lower friction coefficient and a lower wear rate compared to the studied two-component coating ($\text{Al}_2\text{O}_3\text{-ZrO}_2$). The established characteristics reduce the risk of various mechanical damage to the integrity of the coatings with a higher content of TiO_2 .

At the same time, the development of innovative coatings based on modified compositions of the $\text{ZrO}_2\text{-TiO}_2\text{-Al}_2\text{O}_3$ system is of fundamental and applied interest.

The aim of the present work is to study the photoluminescence properties of Sm^{3+} -doped $\text{ZrO}_2\text{-TiO}_2\text{-Al}_2\text{O}_3$ coatings prepared in laboratory conditions. During the analysis and interpretation of the registered emission spectrum (recorded at different excitation wavelengths), experimental data on the structure and characteristics of the prepared experimental coatings were obtained.

2. Experimental Procedure

2.1. Reagents and Materials

Zirconium oxychloride octahydrate ($\text{ZrOCl}_2 \cdot 8\text{H}_2\text{O}$), samarium oxide (Sm_2O_3), alumina (Al_2O_3), titanium(IV) butoxide ($\text{Ti}(\text{OBu})_4$), nitric acid (HNO_3), acetylacetone (AcAc), diethanolamine (DEA), ethanol ($\text{C}_2\text{H}_5\text{OH}$) and deionized water were used as received without further purification. Microscopic glass slides made of soda-lime glass were used as substrates.

2.2. Sol preparation and hydrolysis control

Multicomponent sols were prepared by the sol-gel method. Initially, 8.048 g $ZrOCl_2 \cdot 8H_2O$, 0.527 g Sm_2O_3 and 0.255 g Al_2O_3 were dissolved in ethanol with continuous stirring. Subsequently, 1.1 mL of titanium(IV) butoxide ($Ti(OBu)_4$) was added dropwise under vigorous stirring. Acetylacetonate (AcAc) was used as a chelating agent to control the hydrolysis of the Ti(IV) particles.

After homogenization, hydrolysis of the mixed sol was initiated by adding 85 mL of ethanol, 65 mL of deionized water, 10 mL of nitric acid, and 2.5 mL of AcAc. The resulting sol was stirred for 30 min and then allowed to stand for 24 h at room temperature to ensure stabilization and completion of the sol-gel reactions.

The molar ratios of the precursors in the final solution were as follows:

- Zr : Ti = 27.3 : 1
- Zr : Sm = 43 : 1
- Zr : Al = 87 : 1
- $Ti(OBu)_4$: AcAc \approx 1 : 1.7
- H_2O : (Zr + Ti) \approx 16 : 1
- EtOH : (Zr + Ti) \approx 72 : 1

2.3. Substrate cleaning

The glass substrates were ultrasonically cleaned sequentially in acetone, ethanol and deionized water, followed by air drying.

2.4. Dip coating

Before coating, the sol was filtered through a 0.45 μm PTFE membrane. Thin films were deposited on glass substrates using the dip technique at 25 $^{\circ}C$ and 40–50% relative humidity, with drawing speeds of 72.9 mm/min.

After each deposited layer, the coatings were dried at 100 $^{\circ}C$ for 10 min to remove residual solvent and promote partial gelation. Typically, 3–5 coating layers were applied to obtain films of the desired thickness.

2.5. Thermal treatment

The deposited films were thermally treated in air to obtain transparent multioxide coatings. The heating program consisted of a first stage to 300 $^{\circ}C$ at a heating rate of 1 $^{\circ}C/min$ with a holding time of 1 h, followed by additional heating to 450 $^{\circ}C$ at 2 $^{\circ}C/min$.

3. Results and Discussion

The emission spectrum of the $ZrO_2-TiO_2-Al_2O_3-Sm_2O_3$ coating was recorded at different excitation wavelengths. Under UV excitation ($\lambda_{ex} = 354$ nm), a broad emission band was observed in the region 370–550 nm with a maximum around 420–440 nm (fig.1).

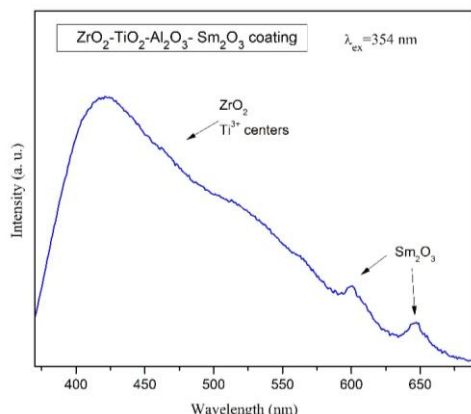


Figure 1. Emission spectrum of deposited $ZrO_2-TiO_2-Al_2O_3-Sm_2O_3$ coating under 354 nm excitation.

Three kinds of different mechanisms have been proposed to explain ZrO_2 blue-green luminescence - an impurity luminescence center model, intrinsic self-trapped excitons and a structure-defect model. [P. Iacconi, D. Lapraz, R. Caruba: Phys. Status Solidi A 50, 275 (1978); M. Garcia-Hipolito, R. Martinez, O. Alvarez-Fregoso: J. Luminesc. 93, 9 (2001); V.A. Emeline, N. Serpone: Chem. Phys. Lett. 345, 105 (2001) 20 W.C. Hsieh, C.S. Su: J. Phys. D: Appl. Phys. 27, 1763 (1994); Liang J, Deng Z, Jiang X, Li F and Li Y 2002 Inorg. Chem. 41 3602]. At present, the generally

accepted model is the structure-defect one, suggesting that the luminescence of ZrO_2 arises from oxygen-vacancy defects (F^+ centers). Thus the observed broad band with a maximum around 420–440 nm can be associated with oxygen vacancies in ZrO_2 together with Ti^{3+} centers.

Sm^{3+} ions are characterized by narrow, sharp emission lines in the wavelength range 500 nm -750 nm, which are attributed to the characteristic intra-configuration f-transition of $Sm^{3+} \ ^5G_{5/2} \rightarrow \ ^7H_J$ where $J = 5/2, 7/2, 9/2, 11/2$. [W.T. Carnall, P.R. Fields, K. Rajnak J. Chem. Phys., 49 (1968), p. 4424; W.T. Carnall, G.L. Goodman, K. Rajnak, R.S. Rana J. Chem. Phys., 90 (1989), p. 3443]. Based on this, the observed weakly intense and narrower emission bands at 600 nm and 647 nm (fig.1.) can be assigned to the $\ ^5G_{5/2} \rightarrow \ ^7H_{7/2}$ and $\ ^5G_{5/2} \rightarrow \ ^7H_{9/2}$ transitions of Sm^{3+} ions.

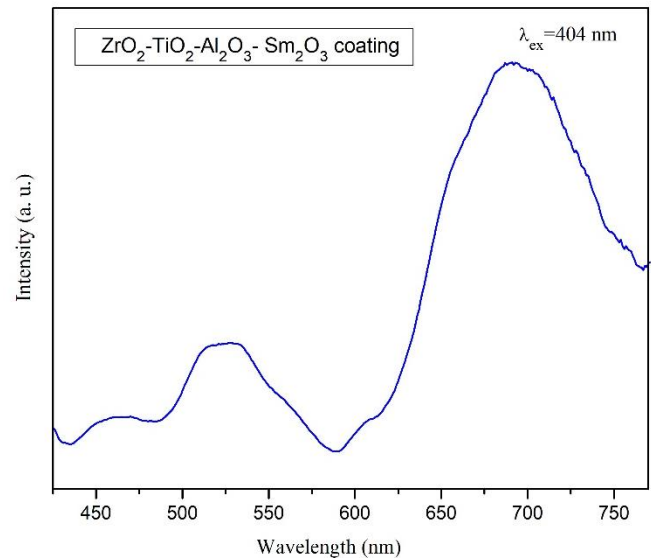


Figure 2. Emission spectrum of deposited $ZrO_2-TiO_2-Al_2O_3-Sm_2O_3$ coating under 404 nm excitation.

When excited with 404 nm the spectral profile changes significantly. A broad emission in the region 500–750 nm is observed with a maximum around 680–710 nm, without clearly pronounced narrow lines characteristic of the $4f-4f$ transitions of Sm^{3+} . This indicates that under these conditions the emission is dominated by defect levels in the oxide coating.

It is clear that the direct luminescence of Sm^{3+} ions, which falls in the same region (680-710 nm), is strongly suppressed and does not dominate the observed emission.

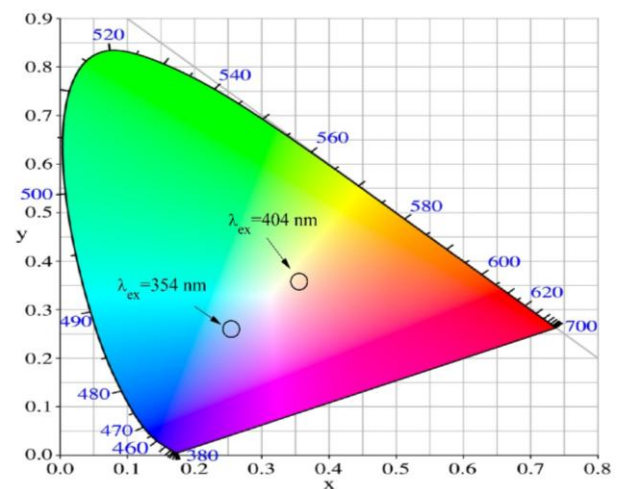


Figure 3. CIE chromaticity diagram of coatings under 354 nm and 404 nm wavelength of excitation.

In order to estimate the actual emitted color, the Commission International de l'Eclairage (CIE) 1931 chromaticity diagram was used [Smith, T.; Guild, J. The CIE colorimetric standards and their use. Trans. Opt. Soc. 1931, 33, 73.]. The chromaticity coordinates

were calculated from the emission spectra by using color calculator software SpectraChroma (CIE coordinate calculator) [Paolini, T.B. SpectraChroma (Version 1.0.1) [Computer Software]. 2021. Available online: <https://zenodo.org/records/4906590> (accessed on 7 June 2021)]. The values of the chromaticity coordinates of the coating excited under 354 nm correspond to the pale pink color of emission (0.252, 0.272) and under 404 nm has orange color of emission (0.353, 0.370).

The color purity of the synthesized samples can also be calculated via chromaticity coordinates of CIE 1931 diagram. The following expression was used:

$$\text{Color purity} = \frac{\sqrt{(x-x_{ee})^2 + (y-y_{ee})^2}}{\sqrt{(x_d-x_{ee})^2 + (y_d-y_{ee})^2}} \cdot 100\% \quad , \quad [\text{book:}$$

Schubert, E. F. (2006). *Light-emitting diodes*, Cambridge university press, p. 300]

where (x,y) represents the color coordinates of the synthesized glasses; (x_{ee}, y_{ee}) is the illuminant point of the 1931 CIE Standard Source C with color coordinates (0.3101, 0.3162); (x_d, y_d) are the chromaticity coordinates of the dominant wavelength point, which were obtained by extending the straight line between the point of (x, y) and the illuminant point (x_{ee}, y_{ee}) to the other side of the chromaticity diagram. Generally, it is accepted that 100 % is for pure color and 0% is for white light. The established values for the color purity of coatings excited by 354 nm wavelength is 26% and for 404 nm is 25%.

Discussion:

The lack of clearly defined linear emission peaks of the active Sm³⁺ ions, even under direct excitation around 404 nm, can be explained by competing non-radiative processes in the oxide coating, as well as by possible concentration quenching and strong interaction between Sm³⁺ ions and defect states of TiO₂/ZrO₂. The broad character of the observed emission is typical of defect-driven luminescence in amorphous or nanocrystalline oxide systems.

The obtained results show that the luminescent properties of the studied coating are determined mainly by the defective structure of the coating, creating prerequisites for further optimization of the composition and thermal treatment in order to activate the emission of rare earth ions.

4. Conclusion

Transparent Sm³⁺-doped ZrO₂-TiO₂-Al₂O₃ coatings were successfully synthesized on glass substrates using a sol-gel dip-coating technique followed by thermal treatment. The applied synthesis approach enabled the formation of homogeneous multicomponent oxide films suitable for optical investigations.

Photoluminescence analysis revealed that the emission properties strongly depend on the excitation wavelength. Under UV excitation at 354 nm, a broad emission band centered at 420–440 nm was observed, which is mainly associated with oxygen-vacancy defects in ZrO₂ and Ti³⁺ centers. Weak emission lines at 600 nm and 647 nm correspond to the characteristic transitions of Sm³⁺ ions. When excited at 404 nm, the emission is dominated by defect-related luminescence in the oxide matrix.

Chromaticity analysis indicated pale pink emission under 354 nm excitation and orange emission under 404 nm excitation. The obtained results demonstrate that the luminescent behavior of the coatings is largely governed by defect states in the oxide structure. Such transparent luminescent coatings may be considered as promising materials for photonic applications and potentially for light management in photovoltaic devices.

5. References

1. T. A. Otitoju, P. U. Okoye, G. Chen, Y. Li, M. O. Okoye, S. Li, Advanced ceramic components: materials, fabrication, and applications, *J. Industrial and Engineering Chemistry* 85, 2020, pp. 34-65.

2. S. A. Kumar, B. A. Viswanath, P. Raghul, A review of preparation and characterization of sol-gel coating for corrosion mitigation, *Int. J. Eng. Technol. Manag. Sci.*, 2 (8), 2024, pp. 11-24.
3. A. Knaislova', D. Horkavcov', E. Jablonska', D. Vojtech, Sol-gel TiO₂-based coatings in 3D printed porous Ti-6Al-4V alloy structures as efficient antibacterial drug delivery systems: Thorough structural and biological characterization, *Applied Surface Science Advances*, 29, 2025, 100816.
4. S. Feliu Jr., F.R. Garcia-Galvan, Corrosion and protection of metallic materials, *Metals*, 15, 346, 2025, pp. 1-8.
5. S. Li, J. Fu, Improvement in corrosion protection properties of TiO₂ coatings by chromium doping, *Corros. Sci.*, 68, 2013, pp. 101-110.
6. M. K. Sahnesarayi, H. Sarpoolaky, S. Rastegari, Effect of heat treatment temperature on the performance of nano-TiO₂ coating in protecting 316L stainless steel against corrosion under UV illumination and dark conditions, *Surf. Coat. Technol.*, 258, 2014, pp. 861-870.
7. X. Shan, L.Q. Wei, P. Liu, X.M. Zhang, W.X. Tang, P. Qian, Y. He, S.F. Ye, Influence of CoO glass-ceramic coating on the antioxidation behavior and thermal shock resistance of 200stainless steel at elevated temperature. *Ceram Int.*, 40 (8), 2014, 12327.
8. Kotlikov E. N., Lavrovskaya N. P., Tenev T. K., Milushev I. K., Aluminum oxide (Al₂O₃) optical films and their applications in the ultraviolet region of the spectrum. *Journal of Optical Technology*, 89, 12, 2022, DOI:10.1364/JOT.89.000752, 752-756.
9. B. C. Wyatt, S. K. Nemani, G. E. Hilmas, E. J. Opila, B. Anasori, Ultra-high temperature ceramics for extreme environments, *Nat. Rev. Mat.*, 2023, pp. 1-17.
10. J. K. B. Balangao, Corrosion of metals: factors, types and prevention strategies. *J. Chem. Health Risks*, 14 (1), 2024, pp. 79-87.
11. I. P. Okokpujie, L. K. Tartibu, H. O. Musa-Basheer, Effect of coatings on mechanical, corrosion and tribological properties of industrial materials: a comprehensive review, *J. Bio. Tribo Corros.* 10, 2024, 2, <https://doi.org/10.1007/s40735-023-00805-1>.
12. D. Barros, I. Vandembulcke, Plasma assisted chemical vapor deposition process for depositing smooth diamond coatings on titanium alloys at moderate temperature, *Diamond Relat. Mater.* 9, 2000, 1862–1866,
13. Cai LF, Zhang YZ, Shi LK. Microstructure and formation mechanism of titanium matrix composites coating onTi-6Al-4 V by laser cladding. *Rare Met.*,26(4), 2027, 342.
14. L. Ceschini, E. Lanzoni, C. Martini, D. Prandstraller, G. Sambogna, Comparison of dry sliding friction and wear of Ti6Al4V alloy treated by plasma electrolytic oxidation and PVD coating, *Wear* 264 (1–2), 2008, 86–95,
15. G. Perumal, M. Geetha, R. Asokamani, N. Alagumurthi, A comparative study on the wear behaviour of Al₂O₃ and SiC coated Ti-6Al-4V alloy developed using plasma spraying technique, *Trans. Ind. Inst. Met.*, 66, 2013, 109–115.
16. H. Li, Y.Z. Sun, J. Zhang, Effect of ZrO₂ particle on the performance of microarc-oxidation coatings on Ti6Al4V. *Appl SurfSci.*, 342, 2015, 183.
17. Y. Wang, G. Darut, T. Poirier, J. Stella, H.L. Liao, M.P. Planche, Ultrasonic cavitation erosion of as-sprayed and laser-remeltedyttria stabilized zirconia coatings. *J Eur Ceram Soc.*, 37(11), 2017, 3623.
18. Song J.B, Choi E, Oh SG, So J, Lee SS, Kim JT, Yun J.Y., Improved reliability of breakdown voltage measurement of yttrium oxide coatings by plasma spray. *Ceram Int.*, 45(17), 2019, 22169.
19. Wang F, Luo GN, Huang JJ, Liu Y. Properties improvement of atmospheric plasma sprayed tungsten coating by annealing. *SurfCoa Technol.*, 358, 2019, 276.
20. V. Ambardekar, P. P. Bandyopadhyay, S. B. Majumder, Hydrogensensing performance of atmospheric plasma sprayed tin dioxide coating. *Int J Hydrogen Energ.* 44(26), 2019, 14092.
21. H. D. Gao, Z. H. Wang, J. Shao, Manufacture and characteristics of Al₂O₃ composite coating on steel substrate by SHS process. *Rare Met.*, 38(7), 2019, 704.

22. N. Kaczmarczyk, J. Szczurek, B. Babiarczuk, P. Gronowicz, M. Paszkowski, M. Kowalski, B. Borak, W. Jones, J. Detyna, J. Krzak, Thin film quality of sol-gel SiO_2 coatings prepared on Ti6Al4V depending on their composition and titanium substrate preparation, *J Mater Sci*, 60, 2025, pp.13974–14004.
23. Sathish Sharma G, Sugavaneswaran M, Vijayalakshmi U, Prakash R. Influence of α -alumina coating on surface properties of direct metal laser sintered 316L stainless steel. *Ceram Int*. 2019;45(10):13456.
24. Kishida S, Ju DY, He H, Li Y. Coating of α - Al_2O_3 on the stainless steel substrate by electrophoretic deposition method. *J Environ Soc Sci*. 2009;21(1):S112.[14] Si TZ, Liu N, Zhang QA, You XQ. Thermal shock fatigue behavior of TiC/ Al_2O_3 composite ceramics. *Rare Met*. 2008;27(3):308.
25. K. P. Misra (ed), R. D. K. Misra (ed), *Ceramic Science and Engineering: Basics to Recent Advancements* (Elsevier Series in Advanced Ceramic Materials), Book, 1st Edition, Elsevier, 2022, 616.
26. N. Karwalo, *Ceramic Engineering*, Book, Discovery Publishing House, 2023, 200.
27. A. Sharma, A. Babbar, Y. Tian, B. P. Pathri, M. Gupta, R. Singh, Machining of ceramic materials: a state-of-the-art review”, *Int. J. on Inter. Des. and Man. (IJIDeM)*, 17(6), 2023, pp. 2891-2911.
28. M. F. Zawrah, M. A. Taha, R. A. Youness, *Advanced Ceramics: Stages of Development*, In advanced ceramics., Springer Nature Switzerland, 2023.
29. Peng-Yue Gao, Yu-Duo Ma, Wen-Wei Sun, Yong Yang, Chen Zhang, Yu-Hang Cui, Yan-Wei Wang, Yan-Chun Dong, Microstructure and properties of Al_2O_3 - ZrO_2 - TiO_2 composite coatings prepared by plasma spraying, *Rare Met.*, 2021, 40(7), pp.1825–1834.
30. Limarga AM, Widjaja S, Yip TH. Mechanical properties and oxidation resistance of plasma-sprayed multilayered $\text{Al}_2\text{O}_3/\text{ZrO}_2$ thermal barrier coatings. *Surf Coat Technol*. 2005;197(1):93.
31. Ito A, You Y, Ichikawa T, Tsuda K, Goto T. Preparation of Al_2O_3 - ZrO_2 nanocomposite films by laser chemical vapour deposition. *J Eur Ceram Soc*. 2014;34(1):155.
32. Chen YD, Yang Y, Chu ZH, Chen XG, Wang L, Liu Z, Dong YC, Yan DR, Zhang JX, Kang ZL. Microstructure and properties of Al_2O_3 - ZrO_2 composite coatings prepared by air plasma spraying. *Appl Surf Sci*. 2018;431, 193.
33. Toma FL, Stahr CC, Berger LM, Saaro S, Herrmann M, Deska D, Michael G. Corrosion resistance of APS- and HVOF-sprayed coatings in the Al_2O_3 - TiO_2 system. *J Therm Spray Technol*. 2010;19(1–2), 137.
34. Fervel V, Normand B, Coddet C. Tribological behavior of plasma sprayed Al_2O_3 -based cermet coatings. *Wear*. 1999; 230(1), 70.
35. Klyatskina E, Espinosa-Fernandez L, Darut G, Segovia F, Salvador MD, Montavon G, Agorges H. Sliding wear behavior of Al_2O_3 - TiO_2 coatings fabricated by the suspension plasma spraying technique. *Tribol Lett*. 2015;59(1):2.
36. Younes R, Bradai MA, Sadeddine A, Mouadji Y, Bilek A, Benabbas A. Effect of TiO_2 and ZrO_2 reinforcements on properties of Al_2O_3 coatings fabricated by thermal flame spraying. *Trans Nonferrous Met Soc China*. 2016;26(5):1345.
37. Jia SK, Zou Y, Xu JY, Wang J, Yu L. Effect of TiO_2 content on properties of Al_2O_3 thermal barrier coatings by plasma spraying. *Trans Nonferrous Met Soc China*. 2015;25(1), 175.
38. K. G. Girisha, K.V. Sreenivas Rao, C. Durga Prasad, Slurry erosion resistance of martensitic stainless steel with plasma sprayed Al_2O_3 -40% TiO_2 coatings. *Mater Today Proc.*, 5(2), 2018, 7388.